Reionization and Galaxy Formation in Warm Dark Matter Cosmologies

Dayal, Pratika; Choudhury, Tirthankar Roy; Bromm, Volker; Pacucci, F.

Published in:
Astrophysical Journal

DOI:
10.3847/1538-4357/836/1/16

Publication date:
2017

The Astrophysical Journal, 836:16 (13pp), 2017 February 10 doi:10.3847/1538-4357/836/1/16

Reionization and Galaxy Formation in Warm Dark Matter Cosmologies

Pratika Dayal[1], Tirthankar Roy Choudhury[2], Volker Bromm[3], and Fabio Pacucci[4]
[1] Kapteyn Astronomical Institute, University of Groningen, P.O. Box 800, 9700 AV Groningen, The Netherlands
[2] National Centre for Radio Astrophysics, Tata Institute of Fundamental Research, Pune 411007, India
[3] Department of Astronomy and Texas Cosmology Centre, University of Texas, Austin, TX 78712, USA
[4] Department of Physics, Yale University, P.O. Box 208121, New Haven, CT 06520, USA
Received 2016 October 27; revised 2016 December 12; accepted 2017 January 4; published 2017 February 6

Abstract

We compare model results from a semi-analytic (merger-tree based) framework for high-redshift ($z \simeq 5$–20) galaxy formation against reionization indicators, including the *Planck* electron scattering optical depth ($\tau_{\rm es}$) and the ionizing photon emissivity ($\dot{n}_{\rm ion}$), to shed light on the reionization history and sources in Cold (CDM) and Warm Dark Matter (WDM; particle masses of $m_x = 1.5$, 3, and 5 keV) cosmologies. This model includes all of the key processes of star formation, supernova feedback, the merger/accretion/ejection driven evolution of gas and stellar mass and the effect of the ultra-violet background (UVB), created during reionization, in photo-evaporating the gas content of galaxies in halos with $M_h \lesssim 10^9\,M_\odot$. We find that the delay in the start of reionization in light (1.5 keV) WDM models can be compensated by a steeper redshift evolution of the ionizing photon escape fraction and a faster mass assembly, resulting in reionization ending at comparable redshifts ($z \simeq 5.5$) in all the dark matter models considered. We find that the bulk of the reionization photons come from galaxies with a halo mass of $M_h \lesssim 10^9\,M_\odot$ and a UV magnitude of $-15 \lesssim M_{\rm UV} \lesssim -10$ in CDM. The progressive suppression of low-mass halos with decreasing m_x leads to a shift in the "reionization" population to larger halo masses of $M_h \gtrsim 10^9\,M_\odot$ and $-17 \lesssim M_{\rm UV} \lesssim -13$ for 1.5 keV WDM. We find that current observations of $\tau_{\rm es}$ and the ultra violet luminosity function are equally compatible with all the (cold and warm) dark matter models considered in this work. Quantifying the impact of the UVB on galaxy observables (luminosity functions, stellar mass densities, and stellar to halo mass ratios) for different DM models, we propose that global indicators including the redshift evolution of the stellar mass density and the stellar mass–halo mass relation, observable with the *James Webb Space Telescope*, can be used to distinguish between CDM and WDM (1.5 keV) cosmologies.

Key words: dark matter – cosmic background radiation – cosmological parameters – dark ages, reionization, first stars – intergalactic medium

1. Introduction

According to the standard Lambda Cold Dark Matter (ΛCDM) cosmological model, the universe consists of three main components: dark energy, cold dark matter (CDM), and baryons with energy densities corresponding to $\Omega_\Lambda = 0.6911$, $\Omega_m = 0.3089$, and $\Omega_b = 0.049$ respectively (Planck Collaboration et al. 2016a). Dark matter forms the basis of the hierarchical model of galaxy formation, providing the halos into which baryonic matter collapses, merging and accreting matter to form successively larger structures through cosmic time. With its property of clustering on all scales, CDM has been remarkably successful in predicting the large-scale structure of the universe, the temperature anisotropies measured by the cosmic microwave background (CMB) and Lyα forest statistics (e.g., Peebles 1971; Bond & Szalay 1983; Blumenthal et al. 1984; Lange et al. 2001; Cole et al. 2005; Hinshaw et al. 2013; Slosar et al. 2013; Planck Collaboration et al. 2014a). However, as recently reviewed by Weinberg et al. (2015), CDM exhibits a number of small-scale problems, including (1) producing halo profiles that are cuspy as opposed to the observationally preferred constant density cores (Navarro et al. 1997; Subramanian et al. 2000), (2) over-predicting the number of satellite and field galaxies as compared to observations—the "missing satellite problem" (Klypin et al. 1999; Moore et al. 1999), (3) predicting massive (Large Magellanic Cloud mass) concentrated Galactic sub-halos inconsistent with observations (e.g., Boylan-Kolchin et al. 2012), and (4) facing difficulties in producing typical disks due to ongoing mergers down to $z \simeq 1$ (Wyse 2001). The limited success of baryonic feedback in solving these small-scale problems (e.g., Boylan-Kolchin et al. 2012; Teyssier et al. 2013) has prompted questions regarding the nature of dark matter itself. Indeed, a popular solution to the small-scale problems in CDM cosmology involves invoking (∼keV) warm dark matter (WDM) particles that erase small-scale power (e.g., Blumenthal et al. 1984; Bode et al. 2001).[5] Particle physics provides compelling motivation for WDM candidates such as sterile neutrinos, which can be as light as $\sim\mathcal{O}(1)$ keV: extensions beyond the Standard Model allow three sterile neutrinos, two of which could be as heavy as 1–10 GeV, with the lightest one being of the order of $\mathcal{O}(1)$ keV. The possibility of sterile neutrinos being a viable dark matter candidate has recently lent support by observations of a 3.5 keV monochromatic line, that might arise from a light sterile neutrino annihilating into photons, from the Perseus galaxy cluster detected using *XMM-Newton* (Boyarsky et al. 2014; Bulbul et al. 2014).

The most stringent astrophysical constraints on the WDM particle mass of $m_x \geqslant 3.3$ keV have been obtained using the low-z ($z \gtrsim 4$) Lyα flux power spectrum (Viel et al. 2013). However, allowing for the intergalactic medium (IGM) temperature-density relation to vary independently as a function of redshift, Garzilli et al. (2015) have obtained a

[5] However, some works caution that the extremely low-mass WDM particles required to make constant density cores prevent the very formation of dwarf galaxies (Macciò et al. 2012; Schneider et al. 2014).

lower bound of $m_x \geqslant 2.2$ keV using the same data. A number of studies have used alternative high-z probes to obtain constraints on the WDM particle mass ranging from $m_x \gtrsim 1.6$ keV using number counts of high-z gamma-ray bursts (de Souza et al. 2013) to $m_x \gtrsim 1$ keV using dwarf spheroidal galaxy observations (de Vega & Sanchez 2010), simultaneously reproducing stellar mass functions and the Tully–Fisher relation for $z = 0$–3.5 galaxies (Kang et al. 2013) and comparing the observed number density of $z \approx 10$ galaxies to that expected from the halo mass function (HMF; Pacucci et al. 2013).

With its property of smearing out small-scale density perturbations, WDM leads to a delay in the assembly of the lowest mass galaxies at early epochs, resulting in a corresponding delay in the appearance of the first metal-free Population III (PopIII) stars. In addition, since low-mass high-z galaxies are believed to be the main sources of reionizing photons in the early universe (e.g., Barkana & Loeb 2001; Ciardi & Ferrara 2005; Choudhury & Ferrara 2007; Choudhury et al. 2008; Bouwens et al. 2015a; Robertson et al. 2015), their delayed and accelerated assembly would naturally lead to a corresponding delay and acceleration in the reionization history. A number of works have used such arguments to constrain the WDM particle mass: Yoshida et al. (2003) have used simulations of PopIII star formation to show that they can yield a maximum electron scattering optical depth of $\tau_{\rm es} \simeq 0.06$ in WDM models with masses as large as $m_x \simeq 10$ keV. While such models could be ruled out using *WMAP* data, this number is in good agreement with the latest *Planck* estimates (Planck Collaboration et al. 2016a, 2016b). Magg et al. (2016) have recently proposed observing the PopIII supernovae (SNe) rate with the forthcoming *James Webb Space telescope* (*JWST*) and the European-Extremely Large Telescope to differentiate between CDM and WDM, and constrain the mass of the latter. Somerville et al. (2003) have used the global star-formation rate density to show that reionization is delayed until $z \simeq 6$ in $m_x \simeq 1.5$ keV models, a result that is broadly consistent with the latest *Planck* results. Yue & Chen (2012) have used a minimum halo mass for star formation embedded in a bubble-model for reionization to show that although WDM can delay the start of reionization, the end might not necessarily be delayed; however, these authors assume a fixed ionizing photon production rate per baryon and do not explicitly model any baryonic physics. Recently, using a constant relation linking the ultra-violet (UV) and ionizing photon production rates to the DM halo mass, Schultz et al. (2014) have ruled out $m_x \lesssim 1.3$ keV; however, even $m_x \simeq 0.8$ keV WDM yields an optical depth consistent with the latest *Planck* results (Planck Collaboration et al. 2014b, 2016b) using their model. Finally, using a semi-analytic model of galaxy formation, where 10% of the baryons that collapsed into halos, before virialization of the outermost DM shell, are converted into stars, Barkana et al. (2001) obtain constraints of $m_x \gtrsim 1.2\,(0.4)$ keV if the star formation efficiency is the same (10 times larger) at high-z as at $z \sim 3$.

This last work is most similar in spirit to our approach, though it does not include gas loss from SN winds, which progressively decreases the gas fraction in galaxies as shown in Dayal et al. (2014a). A major caveat in many of these existing works is their assumption of a cosmology-independent mass-to-light ratio (*M/L*) or ionizing photon production rate-to-mass ratio. However, as shown in Dayal et al. (2014b), the *M/L* ratio sensitively depends on the cosmology considered: a delay in structure formation in WDM models results in a younger stellar population in low-mass halos that, as a result, produces more light per unit stellar mass compared to CDM. The same behavior is expected to hold for the amount of reionization photons produced per unit stellar mass at any cosmic epoch.

Over the past few years, ground- and space-based observations have allowed a statistically significant data set to be collected for $z \simeq 6$–10 Lyman Break galaxies (LBGs; Bouwens et al. 2010, 2011, 2015b; Castellano et al. 2010; McLure et al. 2010, 2013; Oesch et al. 2010, 2013, 2016; Bradley et al. 2012; Bowler et al. 2014, 2015; Atek et al. 2015; Livermore et al. 2016). In this work, our aim is to revisit the constraints allowed on the WDM particle mass by combining these "galaxy" data sets with the latest limits on the cosmological electron scattering optical depth inferred by *Planck*. We build upon a semi-analytic model that traces both the DM and baryonic assembly of high-z ($\simeq$5–15) galaxies, reproducing a number of key observables, presented in Dayal et al. (2014a, 2014b) to show how the reionization history and sources depend on the DM model considered. The strength of the model lies in the fact that in addition to internal feedback from SN (see Section 2.3 Dayal et al. 2014b) our model also includes the effects of "external" feedback (i.e., reionization photo-evaporating gas from DM halos).

The cosmological parameters used in this work correspond to $(\Omega_{\rm m}, \Omega_\Lambda, \Omega_{\rm b}, h, n_s, \sigma_8) = (0.3089, 0.6911, 0.049, 0.67, 0.96, 0.81)$, consistent with the latest results from the *Planck* collaboration (Planck Collaboration et al. 2016a) and we quote all quantities in comoving units unless stated otherwise.

2. Modeling Galaxy Formation and Reionization

In this work, we explore four DM models: CDM and WDM with $m_x = 1.5$, 3 and 5 keV. Although we cite m_x values assuming thermally decoupled relativistic particles, these numbers can be converted into sterile neutrino masses ($m_{\rm sterile\,\nu}$) using the expression (Viel et al. 2005)

$$m_{\rm sterile\,\nu} = 4.43\ {\rm keV}\left(\frac{m_x}{1\ {\rm keV}}\right)^{4/3}\left(\frac{0.1225}{\Omega_m h^2}\right). \quad (1)$$

This yields $m_{\rm sterile\,\nu} = (6.7,\ 16.8,\ 33.3)$ keV corresponding to $m_x = (1.5,\ 3,\ 5)$ keV respectively.

2.1. Merger Trees and the Baryonic Implementation

We now briefly summarize the theoretical model and interested readers are referred to Dayal et al. (2014a, 2014b) for complete details. We construct 400 merger trees starting at $z = 4$, linearly distributed across the halo mass range $\log(M_h/M_\odot) = 9 - 13$ for the four DM models considered. The merger-trees use 320 equal redshift steps ($\Delta z = 0.05$) between $z = 20$ and $z = 4$ with a mass resolution of $M_{\rm res} = 10^8\,M_\odot$ using the modified binary merger tree algorithm with smooth accretion detailed in Parkinson et al. (2008) and Benson et al. (2013). We scale the relative abundances of the merger tree roots to match the $z = 4$ Sheth–Tormen HMF (Sheth & Tormen 1999) and have verified that these yield HMFs in good agreement with the Sheth–Tormen HMF at all z.

We implement the merger trees with baryonic physics including star formation, SN feedback, and the merger/accretion/ejection driven evolution of gas and stellar masses. Our model is based on the simple premise that any galaxy can

form stars with a maximum efficiency (f_*^{ej}) that provides enough energy to expel all the remaining gas, quenching further star formation, up to a threshold value of f_* (see Dayal et al. 2014a). This implies that the effective star formation efficiency ($f_*^{\rm eff}$) is the minimum between f_*^{ej} and f_*. This model has two z- and mass-independent free parameters whose values are selected to match the evolving ultra-violet luminosity function (UV LF): the maximum threshold star-formation efficiency (f_*) and the fraction of SN energy that goes into unbinding gas (f_w). We implement this simple idea proceeding forward in time from the highest merger tree output redshift, $z = 20$. At any z step, the gas mass in a galaxy is determined both by the gas mass brought in by merging progenitors as well as that smoothly accreted from the IGM. A part ($f_*^{\rm eff}$) of this gas forms new stellar mass, $M_*(z)$, with the final gas mass depending on the ratio of the (instantaneous) energy provided by exploding SNs and the potential energy of the halo. Furthermore, at any step, the total stellar mass in a galaxy is the sum of newly formed stellar mass, and that brought in by its progenitors. In this work, we also explore the effects of the ultra-violet background (UVB) in photo-evaporating gas from low-mass halos, impeding their star-formation capabilities, and its impact on both galaxy assembly and reionization as explained in Section 2.2 that follows.

For simplicity, we assume every new stellar population to have a fixed metallicity of $0.05\,Z_\odot$ and an age of $t_0 = 2$ Myr. Using the population synthesis code STARBURST99 (Leitherer et al. 1999), the initial UV luminosity (at $\lambda = 1500$ Å) can be calculated as $L_{\rm UV}(0) = 10^{33.077}$ $(M_*/M_\odot)$ erg s^{-1} Å^{-1} and the initial output of ionizing photons can be calculated as $\dot{n}_{\rm int}(0) = 10^{46.6255}(M_*/M_\odot)$ s^{-1}. Furthermore, the time evolution of these quantities can be expressed as

$$L_{\rm UV}(t) = L_{\rm UV}(0) - 1.33 \log \frac{t}{t_0} + 0.462, \quad (2)$$

$$\dot{n}_{\rm int}(t) = \dot{n}_{\rm int}(0) - 3.92 \log \frac{t}{t_0} + 0.7. \quad (3)$$

For any galaxy along the merger tree the UV luminosity and ionizing photon output rate are the sum of the values from the new starburst and the contribution from older populations accounting for the drop with time.

As shown in Dayal et al. (2014a, 2014b), our model reproduces the observed UV LF for all DM models (CDM and WDM with $m_x = 1.5$, 3 and 5 keV) at $z \simeq 5$–10 over 7 magnitudes in luminosity and predicts the z-evolution of the faint end UV LF slope, in addition to reproducing key observables including the stellar mass density (SMD) and M/L using fiducial parameter values of $f_* = 0.038$ and $f_w = 0.1$. We maintain these fiducial parameter values in all the calculations carried out in this work.

2.2. Modeling Reionization

The reionization history, expressed through the evolution of the volume filling fraction ($Q_{\rm II}$) for ionized hydrogen (H II), can be written as (Shapiro & Giroux 1987; Madau et al. 1999)

$$\frac{dQ_{\rm II}}{dz} = \frac{dn_{\rm ion}}{dz}\frac{1}{n_{\rm H}} - \frac{Q_{\rm II}}{t_{\rm rec}}\frac{dt}{dz}, \quad (4)$$

where the first term on the right-hand side represents the growth of H II regions, while the second term accounts for the decrease in $Q_{\rm II}$ due to recombinations. Here, $dn_{\rm ion}/dz = f_{\rm esc} dn_{\rm int}/dz$ represents the hydrogen ionizing photon rate density (per comoving volume) contributing to reionization, with $f_{\rm esc}$ accounting for the fraction of ionizing photons that escape out of the galactic environment. Furthermore, $n_{\rm H}$ is the comoving hydrogen number density, $dt/dz = [H(z)(1+z)]^{-1}$ and $t_{\rm rec}$ is the recombination time that can be expressed as (e.g., Madau et al. 1999)

$$t_{\rm rec} = \frac{1}{\chi\, n_{\rm H}\,(1+z)^3 \alpha_{\rm B}\, C}. \quad (5)$$

Here $\alpha_{\rm B}$ is the hydrogen case-B recombination coefficient, $\chi = 1.08$ accounts for the excess free electrons arising from singly ionized helium and C is the IGM clumping factor. We use the results of Pawlik et al. (2009) and Haardt & Madau (2012) who show that the UVB generated by reionization can act as an effective pressure term, reducing the clumping factor with z such that

$$C = \frac{\langle n_{\rm H\,II}^2 \rangle}{\langle n_{\rm H\,II} \rangle^2} = 1 + 43\, z^{-1.71}. \quad (6)$$

While reionization is driven by the hydrogen ionizing photons produced by early galaxies, the UVB built up during reionization suppresses the baryonic content of galaxies by photo-heating/evaporating gas at their outskirts (Klypin et al. 1999; Moore et al. 1999; Somerville 2002), suppressing further star formation and slowing down the reionization process. In order to account for the effect of UVB feedback on $\dot{n}_{\rm ion}$, in the fiducial model, we assume total photo-evaporation of gas from halos below $M_{\rm min} = 10^9\, M_\odot$ embedded in ionized regions at any z; we vary this limit between $M_{\rm min} = 10^{8.5\text{–}9.5}\, M_\odot$ to check the robustness of our results. In this "maximal external feedback" scenario, halos below $M_{\rm min}$ in ionized regions neither form stars nor contribute any gas in mergers. The globally averaged $\dot{n}_{\rm ion}$ can then be expressed as

$$\dot{n}_{\rm ion}(z) = f_{\rm esc}\,[Q_{\rm II}(z)\dot{n}_{\rm II}(z) + [1 - Q_{\rm II}(z)]\dot{n}_{\rm I}(z)], \quad (7)$$

where $\dot{n}_{\rm II}$ and $\dot{n}_{\rm I}$ account for the intrinsic hydrogen ionizing photon production rate density within ionized and neutral regions respectively. While $\dot{n}_{\rm I}$ contains contribution from all sources, $\dot{n}_{\rm II}$ represents the case where sources below $M_{\rm min}$ do not contribute to the ionizing photon budget. At the beginning of the reionization process, the volume filled by ionized hydrogen is very small ($Q_{\rm II} \ll 1$) and most galaxies are not affected by the UVB, so that $\dot{n}_{\rm ion}(z) \approx f_{\rm esc}\,\dot{n}_{\rm I}(z)$. As $Q_{\rm II}$ increases and reaches a value of $\simeq$1, all galaxies less massive than $M_{\rm min}$ are feedback suppressed so that $\dot{n}_{\rm ion}(z) \approx f_{\rm esc}\,\dot{n}_{\rm II}(z)$.

Given that $\dot{n}_{\rm ion}(z)$ is an output of the model, with $t_{\rm rec}$ calculated as a function of z, $f_{\rm esc}$ is the only free parameter in our reionization calculations. In this work, $f_{\rm esc}$ is assumed to be independent of the halo mass. As shown in Section 3 that follows, simultaneously fitting to observations of the CMB electron scattering optical depth ($\tau_{\rm es}$) and the ionizing emissivity require a z-dependent $f_{\rm esc}$.

3. Reionization in Different DM Cosmologies

We now discuss model constraints on m_x using observed values of the CMB electron scattering optical depth ($\tau_{\rm es}$) and ionizing emissivity ($\dot{n}_{\rm ion}$). We then present the corresponding

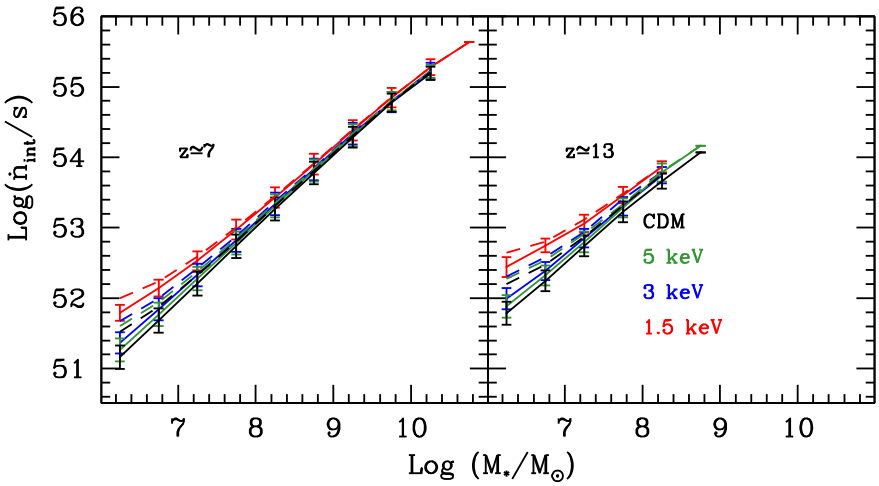

Figure 1. Intrinsic production rate of hydrogen ionizing photons as a function of the stellar mass at $z \simeq 7$ and 13 in the left and right panels, respectively. In each panel, the solid lines show results considering SN feedback only; dashed lines show results considering both SN and UV feedback in the fiducial model ($M_{\rm gas} = 0$ for $M_h \lesssim 10^9\,M_\odot$ halos). The $1-\sigma$ error bars for each M_* bin are plotted for the SN-feedback only scenario. While $\dot{n}_{\rm int}$ scales with the stellar mass in all DM models, 1.5 keV galaxies produce more ionizing photons per unit stellar mass as a result of their younger stellar populations. Including the effects of UV, feedback suppresses star formation in low-mass halos resulting in a lower final stellar mass; however, the final $\dot{n}_{\rm int}$ value, which depends on the latest burst of stars formed, remains unaffected (see Section 3.1 for details).

Table 1
For Each of the DM Models Considered (Column 1), We Show the Redshift Evolution of the Intrinsic Production Rate of Hydrogen Ionizing Photons (Column 5) for Different UV Magnitude Limits (Column 4) in the Presence of Both SN and UVB Feedback (Columns 2 and 3)

DM Model	SN Feedback	UVB Feedback	UV Cut	$\dot{n}_{\rm int}$–z Relation
CDM	yes	yes	all galaxies (Equation (10))	$\log(\dot{n}_{\rm int}) = -0.0036z^2 - 0.058z + 52$
3 keV WDM	yes	yes	all galaxies (Equation (10))	$\log(\dot{n}_{\rm int}) = -0.0088z^2 - 0.037z + 52$
1.5 keV WDM	yes	yes	all galaxies (Equation (10))	$\log(\dot{n}_{\rm int}) = -0.026z^2 - 0.13z + 52$
CDM	yes	yes	$M_{\rm UV} \lesssim -17.7$	$\log(\dot{n}_{\rm int}) = -0.0036z^2 - 0.058z + 52$
3 keV WDM	yes	yes	$M_{\rm UV} \lesssim -17.7$	$\log(\dot{n}_{\rm int}) = -0.021z^2 - 0.004z + 52$
1.5 keV WDM	yes	yes	$M_{\rm UV} \lesssim -17.7$	$\log(\dot{n}_{\rm int}) = -0.033z^2 + 0.17z + 52$

reionization history and sources for both CDM and WDM, as described in what follows.

3.1. Ionizing Photon Production Efficiency in Different DM Cosmologies

The delay in structure formation in WDM models results in a much younger stellar population hosted by low-mass halos at any z, when compared to CDM. This naturally results in low-mass WDM halos producing more ionizing photons, both considering and ignoring the effects of the UVB. This is the behavior shown by $\dot{n}_{\rm int}$ as a function of stellar mass, M_*, in Figure 1. We start by focusing on the left panel corresponding to $z \simeq 7$, where the $\dot{n}_{\rm int}$–M_* relation is essentially independent of the underlying DM model for galaxies with $M_* \gtrsim 10^9\,M_\odot$, corresponding to currently observed LBGs. However, given their younger ages, galaxies with $M_* \simeq 10^{6.2}\,M_\odot$ produce about four times more ionizing photons in the 1.5 keV WDM model as compared to CDM. Quantitatively, we find that $\log(\dot{n}_{\rm int}) = 0.88\log(M_*) + 46$ for the 1.5 keV scenario, steepening to $\log(\dot{n}_{\rm int}) = \log(M_*) + 45$ for CDM, as also quantified in Table 1; while the exact coefficients change, the same trends are seen at $z \simeq 13$ (right panel of the same figure).

According to the fiducial model, including the effects of the UVB results in a loss of all gas content, switching-off star formation in all halos with $M_h \lesssim 10^9\,M_\odot$. This naturally results in a lower stellar mass for the successors of such systems. On the other hand, $\dot{n}_{\rm int}$ effectively only depends on the ongoing star-formation rate (i.e., the instantaneous gas mass) given its steep decay with time as shown in Equation (3). As noted in Dayal et al. (2014a), galaxies with $M_h \lesssim 10^9\,M_\odot$ are feedback limited, contributing only stellar mass but no gas mass to their successors. Thus, although the final stellar mass decreases in the presence of the UVB, $\dot{n}_{\rm int}$ remains unchanged, resulting in a higher $\dot{n}_{\rm int} - M_*$ relation as seen from the same figure. With the largest number of low-mass halos, the effect of UVB suppression is most strongly seen in the CDM, where $M_* \simeq 10^{6.2}\,M_\odot$ halos produce about 2–2.5 times more ionizing photons as compared to the case with SN-feedback only; the effect of the UVB is the weakest in the 1.5 keV case, where $\dot{n}_{\rm int}$ only increases by a factor of 1.5 for low-mass galaxies. Quantitatively, the $\dot{n}_{\rm int} - M_*$ relation including the UVB is well-fit by $\log(\dot{n}_{\rm int}) = 0.95\log(M_*) + 46$ for CDM, changing to $\log(\dot{n}_{\rm int}) = 0.85\log(M_*) + 47$ for the 1.5 keV scenario. Again, galaxies at $z \simeq 13$ follow the same qualitative trends.

3.2. Joint Reionization Constraints from the CMB Optical Depth and UVB Emissivity

Combining *Planck* polarization measurements with temperature and lensing data, the electron scattering optical depth corresponds to $\tau_{\rm es} = 0.066 \pm 0.016$ (Planck Collaboration et al. 2016a), compared to the value of $\tau_{\rm es} = 0.089^{+0.012}_{-0.014}$ obtained by combining *Planck* and *WMAP* low-l polarization data (Planck Collaboration et al. 2014b); low multipole EE data has been used to infer an even lower value of

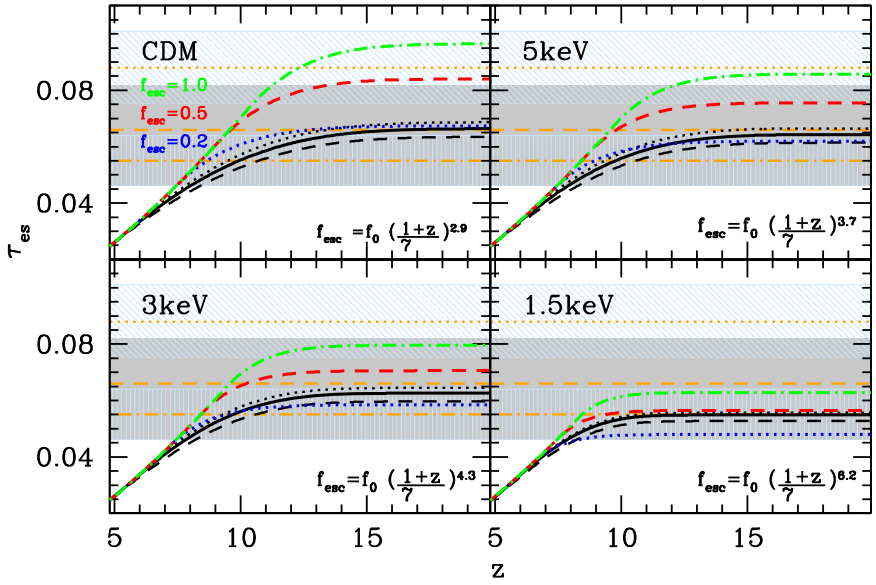

Figure 2. CMB electron scattering optical depth (τ_{es}) as a function of redshift for the four DM models considered in this paper, as marked. In each panel, lines show results using four different values of $f_{esc} = 1.0$ (dotted–dashed green line), 0.5 (dashed red line), 0.2 (dotted blue line), and the fiducial z-dependent value marked (solid black line). The dotted and dashed black lines show results using the fiducial z-dependent f_{esc} value marked, but for a minimum reionization suppressed halo masses of $M_{min} = 10^{8.5}\,M_{\odot}$ and $M_{min} = 10^{9.5}\,M_{\odot}$, respectively; these show that varying M_{min} within one order of magnitude does not change our results appreciably. The z-dependent f_{esc} value has been obtained by simultaneously fitting to τ_{es} and ionizing photon emissivity observations (see Section 3.2). The horizontal dashed line shows the central value for τ_{es} inferred by Planck combining polarization, temperature, and lensing data (Planck Collaboration et al. 2016a) with the gray shaded region showing the $1-\sigma$ errors. The horizontal dotted and dotted–dashed orange lines show the central value for τ_{es} inferred by *Planck* (2014) and *Planck* (2016), respectively; the inclined and vertically shaded (blue) regions show the associated $1-\sigma$ error bars. As seen, while the *Planck*-2014 results ruled out WDM as light as 1.5 keV, though requiring a very steep z-evolution of f_{esc}, this WDM model is allowed by the latest *Planck* (2015, 2016) results.

$\tau_{es} = 0.055 \pm 0.009$ (Planck Collaboration et al. 2016b). We calculate τ_{es} as a function of z by solving the equation

$$\tau_{es}(z) = \sigma_T c \int_0^z dt\; n_e (1+z)^3 \qquad (8)$$

,where $n_e(z) = Q_{II}(z) n_H$ is the global average comoving value of the electron number density and $\sigma_T = 6.6524 \times 10^{-25}$ cm^2 is the Thomson scattering cross-section. $f_{esc}(z)$ governs the evolution of Q_{II} as shown by Equations (4)–(7).

A second observable that needs to be fit simultaneously is the emissivity of ionizing photons, which has been measured for $z \lesssim 6$. In this work, we follow the approach of Kuhlen & Faucher-Giguere (2012) and combine the observational constraints on the H I photoionization rate ($\Gamma_{H\,I}$) from Wyithe & Bolton (2011) with the mean-free path of ionizing radiation (λ_{mfp}) from Songaila & Cowie (2010) to obtain the observational estimate of $\dot{n}_{ion}$. We have used the fiducial values from Kuhlen & Faucher-Giguere (2012): $\gamma = 1$ for the source spectral index and $\beta = 1.3$ for the H I column density distribution. Varying these within allowed limits would only result in larger error bars, leaving our results unchanged (see Kuhlen & Faucher-Giguere 2012).

Once the parameters related to the galaxy formation model are fixed, our model contains only one additional free parameter, f_{esc}, that can be varied to fit the two observational constraints mentioned above. Unfortunately, there do not exist observations of f_{esc} at high redshifts that can be used as possible prior bounds. The indirect constraints on f_{esc} (e.g., Mitra et al. 2013; Robertson et al. 2015) have been obtained only for the standard CDM model and may not be valid for WDM cosmologies. We thus conservatively allow f_{esc} to take any value between 0 and 1 and constrain it by simultaneously fitting τ_{es} and $\dot{n}_{ion}$ for each DM model.

We start by assuming f_{esc} to have a redshift-independent constant value for all the DM models considered (e.g., Schultz et al. 2014). As shown in Figure 2, the *Planck* 2014 value of $\tau_{es} = 0.089^{+0.012}_{-0.014}$ (Planck Collaboration et al. 2014b) requires $f_{esc} \gtrsim 0.5$ for the CDM and 5 keV models and $f_{esc} \sim 1$ for the 3 keV scenario; the 1.5 keV model can be ruled out using this data since it results in an optical depth lower than these *Planck* limits even in the maximal case of $f_{esc} = 1$. The lower *Planck* 2015 value of $\tau_{es} = 0.066 \pm 0.016$ is well-reproduced for CDM and $m_x \lesssim 3$ keV WDM models for $f_{esc} \simeq 0.2$; the 1.5 kev case requires a higher value of $f_{esc} \gtrsim 0.5$ to be consistent with the observed bounds. We note that the most recent, and lowest, value of $\tau_{es} = 0.055 \pm 0.009$ (Planck Collaboration et al. 2016b) is matched by all DM models for f_{esc} values as low as 20%.

Although matching the observed τ_{es}, even the minimum z-independent constant value of $f_{esc} = 0.2$ over-predicts the observed value of $\dot{n}_{ion}$ by about 0.8 dex at $z \simeq 6$ as shown in Figure 3. A scenario wherein f_{esc} is z-independent is therefore ruled out by the emissivity constraints, irrespective of the DM model considered. In what follows, we show results using f_{esc} calibrated to the *Planck* 2015 results (Planck Collaboration et al. 2016a) that has been obtained combining polarization, lensing, and temperature data; however, these results are within the error bars and hence also valid for the latest *Planck* 2016 estimates as shown in Figure 2.

Reconciling the optical depth and emissivity data sets requires a z-dependent value of f_{esc} such that

$$f_{esc}(z) = \min\left[1,\; f_0\left(\frac{1+z}{7}\right)^{\alpha}\right] \quad (z \geqslant 5), \qquad (9)$$

where f_0 and α are z-independent parameters, whose values are determined individually for each DM model considered, the

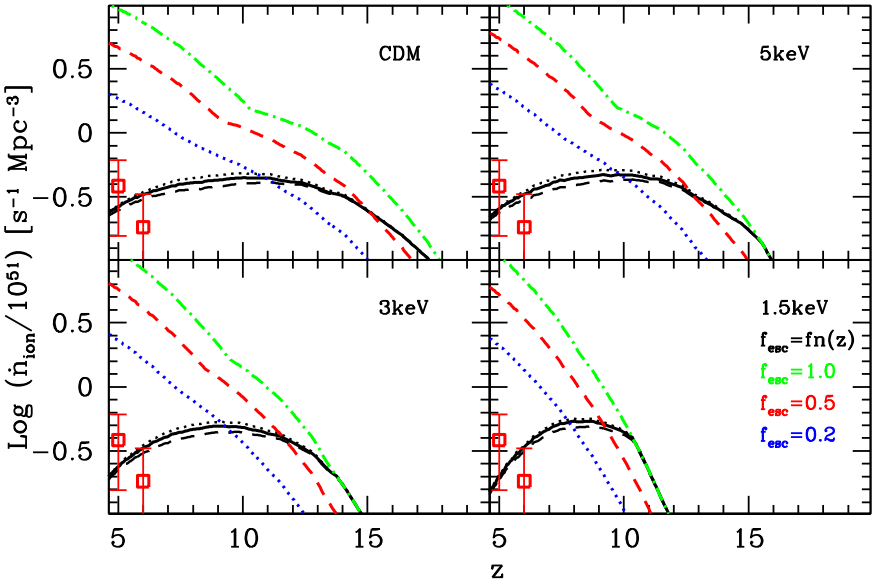

Figure 3. Redshift evolution of the H I ionizing photon emissivity for the four DM models considered in this paper, as marked. In each panel, lines show results using four different values of $f_{\rm esc} = 1.0$ (dotted–dashed green line), 0.5 (dashed red line), 0.2 (dotted blue line), and the fiducial z-dependent value (solid line). The dotted and dashed black lines show results using the fiducial z-dependent value marked, but for $M_{\rm min} = 10^{8.5}\,M_{\odot}$ and $M_{\rm min} = 10^{9.5}\,M_{\odot}$, respectively, to show that varying $M_{\rm min}$ by one order of magnitude does not change our results appreciably. As seen, a constant $f_{\rm esc}$ value severely over-predicts $\dot{n}_{\rm ion}$ compared to the observations (points) at $z \simeq 5$, 6 in all DM models. The observational results (and associated error bars) have been calculated following the approach of Kuhlen & Faucher-Giguere (2012), i.e., by combining the observational constraints on $\Gamma_{\rm H\,I}$ from Wyithe & Bolton (2011) with the mean-free path for ionizing photons ($\lambda_{\rm mfp}$) from Songaila & Cowie (2010). See Section 3.2 for details.

Table 2
The Parameter Values for the z-evolution of the Escape Fraction ($f_{\rm esc}$) for different DM Models Using *Planck* 2015 Data that Combines Polarization, Lensing, and Temperature Data; the Numbers in Brackets Show the Sterile Neutrino Mass Corresponding to m_x

Model	$f_0 \times 100$	α
CDM	4.5	2.9
$m_x = 5$ keV (33.3 keV)	4.1	3.7
$m_x = 3$ keV (16.8 keV)	3.8	4.3
$m_x = 1.5$ keV (6.7 keV)	4.8	6.2

Note. The z-dependence of $f_{\rm esc}$ is taken to be $f_{\rm esc}\,(z) = f_0\,[(1+z)/7]^{\alpha}$.

results of which are shown in Table 2. This formalization requires $\alpha > 0$, which provides enough photons at high-z to obtain the right value of $\tau_{\rm es}$, while yielding reasonably low $\dot{n}_{\rm ion}$ values at later times; this point has already been noted in previous works (see, e.g., Mitra et al. 2011, 2012). With the largest number of low-mass halos available to provide H I ionizing photons, CDM requires the most shallow z-dependence on $f_{\rm esc}$. A decrease in the number of low-mass halos with decreasing m_x requires successively larger $f_{\rm esc}$ values at early times, resulting in a steeper z-dependence. Finally, varying the minimum halo mass below which the UVB photo-evaporates the entire gas content by an order of magnitude between $10^{8.5}$ to $10^{9.5}\,M_{\odot}$ has a minimal effect on both $\tau_{\rm es}$ and $\dot{n}_{\rm ion}$: as seen from Figure 2, while $\tau_{\rm es}$ changes by 0.005, $\dot{n}_{\rm ion}$ changes by less than 0.1 dex. For this reason, we only show results for the fiducial value of $M_{\rm min} = 10^{9}\,M_{\odot}$ in what follows.

We end by noting that while the older *Planck* (2014) results could have ruled out the 1.5 keV scenario, all models are equally probable given the latest CMB results (Planck Collaboration et al. 2016a, 2016b), though the 1.5 keV model requires an exceptionally steep z-evolution of $f_{\rm esc}$.

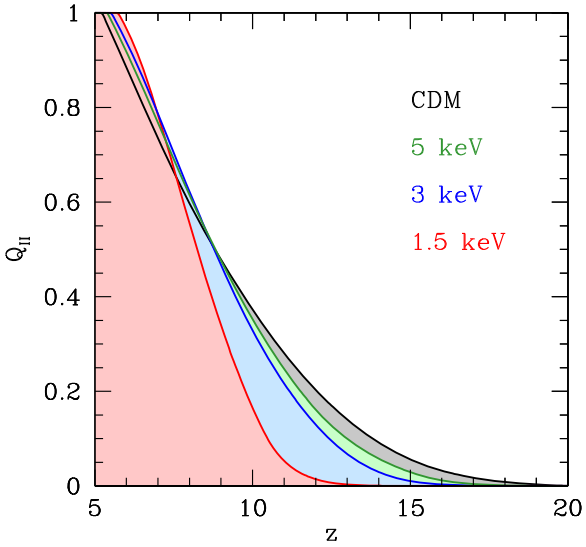

Figure 4. Volume filling fraction of ionized hydrogen as a function of z for the fiducial parameter values for all four DM models considered in this work. While reionization starts at comparable epochs in CDM and $m_x \gtrsim 3$ keV, the suppression of small-scale structure leads to a delay in reionization, by about 150 Myr, for 1.5 keV WDM. However, a combination of accelerated galaxy assembly and a steeper $f_{\rm esc}$–z relation in 1.5 keV WDM models result in reionization ending at comparable redshifts in all models.

3.3. Reionization Histories and Sources in Different DM Models

As discussed in Section 2.2, given the source galaxy population derived from the semi-analytic model, the reionization history, expressed through the global z-evolution of $Q_{\rm II}$, is fixed once $f_{\rm esc}(z)$ is determined. Given that CDM allows halo collapse on the smallest scales, it is the most affected by UVB feedback; the effect of UVB feedback naturally decreases with a decrease in the WDM particle mass. As shown in Figure 4,

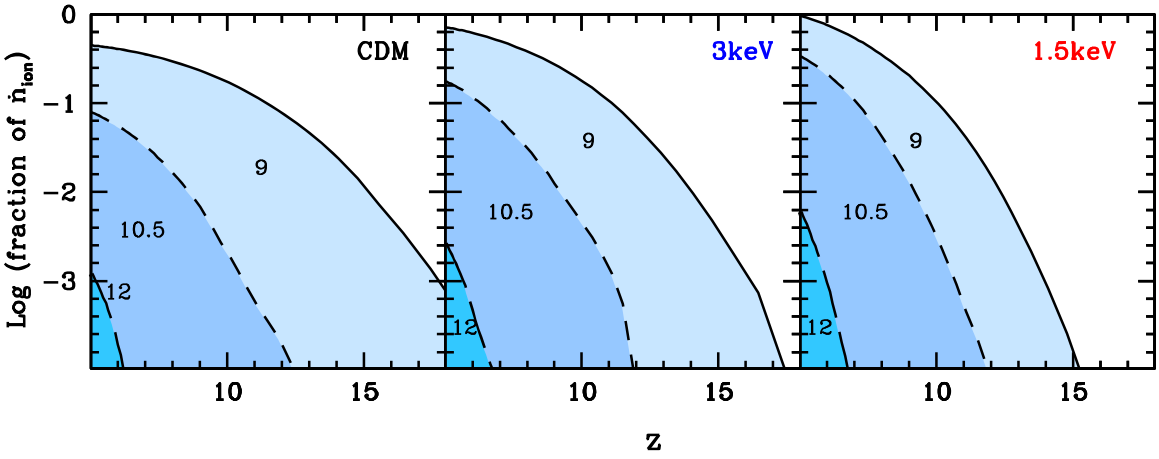

Figure 5. Fractional contribution from galaxies of halo masses $M_h \gtrsim 10^9$, $10^{10.5}$, and $10^{12}\,M_\odot$, as marked, for CDM (left panel), 3 keV (middle panel), and 1.5 keV WDM (right panel). As seen, galaxies with $M_h \gtrsim 10^9\,M_\odot$ provide about 40% of the total ionizing budget, with the rest coming from lower mass halos in the CDM. However, as a result of suppression of structure formation on small scales, these galaxies provide all of the ionizing photon budget in the 1.5 keV model. As expected, the contribution drops steeply with an increase in the halo mass such that $M_h \gtrsim 10^{12}\,M_\odot$ galaxies contribute negligibly to the ionizing budget for all of the DM models considered.

reionization starts with the formation of the first galaxies as early as $z \simeq 18$ in CDM, corresponding to about 200 Myr after the big bang and is 50% complete by $z \simeq 9$, initially driven by low-mass $M_h \lesssim M_{\rm min}$ halos (see also Bromm & Yoshida 2011). Progressive UVB suppression of such halos with decreasing z then results in $M_h \gtrsim M_{\rm min}$ halos providing most of the H I ionizing photons and reionization is 90% complete by volume at $z \simeq 6$.

Reionization is delayed by a small period of about 60 Myr in $m_x \gtrsim 3$ keV models compared to CDM as shown in the same figure. However, this minor delay is easily compensated by the steeper $f_{\rm esc}$ behavior (see Table 2) such that reionization is 50% and 90% complete at almost the same epochs as in CDM, at $z \simeq 8.5$ and 6 respectively. With its largest suppression of low-mass halos, reionization only starts at $z \simeq 12$ in the 1.5 keV scenario, being delayed by about 150 Myr compared to CDM. This delay in the start of reionization is compensated by (1) the larger, and hence less feedback limited, galaxies that produce stars and H I ionizing photons at a much faster rate as compared to CDM and $m_x \gtrsim 3$ keV models, and (2) the steeper $f_{\rm esc}$ evolution required to match to the observed optical depth and emissivity constraints. The two effects results in a faster reionization in the 1.5 keV model, which is 90% complete by $z \simeq 6.5$. Interestingly, reionization finishes by about $z \simeq 5.5$ in all of these different scenarios, in accordance with the results of Yue & Chen (2012) who have shown that, although WDM can delay the start of reionization, the end is not necessarily delayed.

With regards to the main reionization sources, we now calculate the fractional contribution of galaxies to the total ionizing emissivity at $z \simeq 5$ as a function of their halo masses and magnitudes. Given the similarity between CDM and 5 keV demonstrated above, for clarity, we only show results for CDM, 3 keV and 1.5 keV WDM in what follows. As a function of halo mass, we find that CDM galaxies with $M_h \gtrsim 10^9\,M_\odot$ provide only about 40% of the total ionizing photons, with the dominant contribution coming from lower halo masses as shown in Figure 5. Furthermore, $M_h \gtrsim 10^{10.5}\,M_\odot$ halos only provide ~8% of the total ionizing photons, dropping to less than 0.1% for $M_h \gtrsim 10^{12}\,M_\odot$ halos. Given 3 keV WDM suppresses the formation of low-mass halos, $M_h \gtrsim 10^9\,M_\odot$ galaxies provide about 63% of the total ionizing photons, with $M_h \gtrsim 10^{10.5}$ (10^{12}) $M_\odot$ halos contributing only 15% (0.3%) to the total ionizing budget. With the suppression of all halos below $\simeq 10^9\,M_\odot$, galaxies above this limit make up 100% of the ionizing photon budget in the 1.5 keV WDM model, with $M_h \gtrsim 10^{10.5}\,M_\odot$ halos providing an appreciable 32% of the total budget.

In terms of the observed UV magnitude, we find that an integration limit as faint as $M_{\rm UV} = -10$ is required in order to catch the total ionizing photon budget for CDM and the 3 keV WDM models as shown in Figure 6; integrating down to the generally used limit of $M_{\rm UV} = -13$ provides 63% of the budget for CDM, rising to about 80% for the 3 keV scenario, with the rest coming from fainter sources. Given the lack of low-mass halos, on the other hand, galaxies brighter than $M_{\rm UV} = -13$ provide all of the ionizing budget for the 1.5 keV model. As expected from the discussion above, massive galaxies brighter than $M_{\rm UV} = -17$ that reside in $M_h \gtrsim 10^{10.5}\,M_\odot$ halos (see Figure 3; Dayal et al. 2014a) provide only about 10% of the total ionizing budget in CDM. This rises to about 20% (40%) for the three (1.5) keV models.

To summarize, we find the that bulk of the reionization photons comes from galaxies with $M_h \lesssim 10^9\,M_\odot$ and $-15 \lesssim M_{\rm UV} \lesssim -10$ in CDM. The progressive suppression of low-mass halos with decreasing m_x leads to a shift in the "reionization" population to larger halo masses of $M_h \gtrsim 10^9\,M_\odot$ and $-17 \lesssim M_{\rm UV} \lesssim -13$ for 1.5 keV WDM.

4. Reionization Impact on High-z Galaxy Observables

We now quantify the impact of the UVB feedback on global observables such as the UV LF, the SMD, and the ionizing photon density, as well as observables measured for individual galaxies such as the stellar mass–halo mass relation. Given the small impact of changing $M_{\rm min}$ between $10^{8.5}$ and $10^{9.5}\,M_\odot$ on reionization noted in Section 3.2, we only show results for the fiducial case of $M_{\rm min} = 10^9\,M_\odot$ in what follows.

4.1. Faint End of the UV Luminosity Functions

The evolving UV LF has now been measured over an unprecedented 10 (7) magnitudes at $z \simeq 7$ (8) as shown in

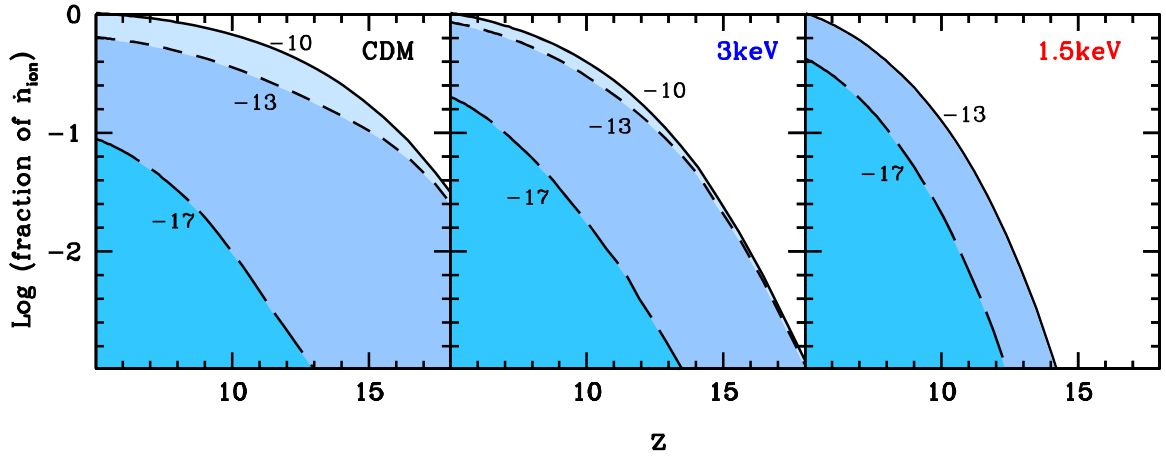

Figure 6. Fractional contribution from galaxies integrating down to UV magnitudes $M_{\rm UV} = -10$, -13, and -17, as marked, for CDM (left panel), 3 keV (middle panel), and 1.5 keV WDM (right panel); given the lack of low-mass halos, there are no galaxies fainter than $M_{\rm UV} = -13$ in the 1.5 keV WDM. As seen, while currently observed galaxies with $M_{\rm UV} \lesssim -17$ provide about 10% of the total ionizing photon budget in CDM, this rises to about 40% in the 1.5 keV scenario. Furthermore, we find that while an integration limit of $M_{\rm UV} = -13$ suffices for 1.5 keV WDM, a fainter limit of $M_{\rm UV} = -10$ is required to catch all of the reionization photons for CDM and $m_x \gtrsim 3$ keV WDM.

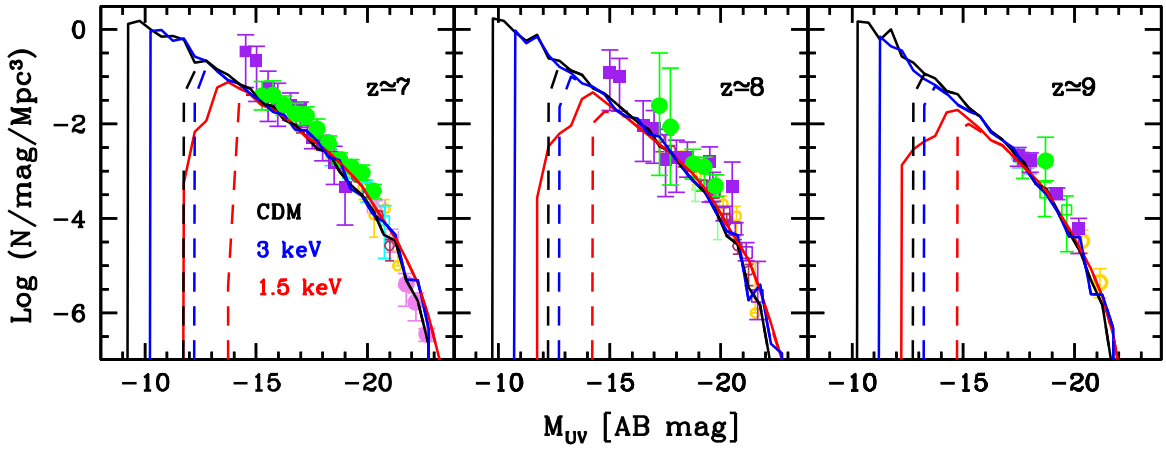

Figure 7. Evolving LBG UV LFs at $z \simeq 7$ (left panel), 8 (central panel), and 9 (right panel) for CDM, 3 keV and 1.5 keV WDM, as marked. In each panel, solid and dashed lines show results for SN feedback and the fiducial model (SN and UV feedback), respectively. As seen, results from models with and without UV feedback are in agreement for all DM models, and with the observations, down to $M_{\rm UV} \simeq -14$. In all panels, points show observational results: (a) $z \simeq 7$: Oesch et al. (2010, empty cyan squares), Bouwens et al. (2011, empty yellow circles), Castellano et al. (2010, empty purple triangles), McLure et al. (2010, empty red triangles), McLure et al. (2013, empty maroon circles), Bowler et al. (2014, filled purple circles), Atek et al. (2015, filled green circles) and Livermore et al. (2016, filled purple squares); (b) $z \simeq 8$: Bouwens et al. (2011, empty yellow circles), Bradley et al. (2012, empty purple squares), McLure et al. (2013, empty maroon circles), Atek et al. (2015, filled green circles) and Livermore et al. (2016, filled purple squares) and (c) $z \simeq 9$: Zheng et al. (2012, filled green circle), McLure et al. (2013, empty blue circles), Oesch et al. (2013, empty green squares), McLeod et al. (2016, filled purple squares) and Bouwens et al. (2016, empty yellow circles).

Figure 7. At $z \simeq 7$ and 8, the faint end ($M_{\rm UV} \gtrsim -16$) data has been collected using the lensed Hubble Frontier fields (HFF; Atek et al. 2015; Livermore et al. 2016), while the brightest galaxies have been detected using ground-based Ultra-Vista surveys (e.g., Bradley et al. 2014; Bowler et al. 2014); (unlensed) *HST* data has been used to obtain the $z \simeq 9$ UV LF as shown in the same figure.

We start by discussing the UV LF considering only internal (SN) feedback; this effectively implies setting $M_{\rm min} = 0$ when modeling the feedback effects of the UVB. As shown, the UV LFs for CDM and 3 keV WDM are in agreement at least down to $M_{\rm UV} \simeq -11$ at $z \simeq 7$–9; results from the 1.5 keV scenario are in agreement with these down to $M_{\rm UV} \simeq -12$ at $z \simeq 7$ and start peeling-away at a slightly brighter magnitude corresponding to $M_{\rm UV} \simeq -15$ at $z \simeq 9$ (see also Dayal et al. 2014b). However, within error bars, all three UV LFs are in agreement with observations over the entire range probed so far. As shown in Dayal et al. (2014b), this overlap is the result of the absence of low-mass halos in WDM models being partly compensated by their younger, and hence brighter, stellar populations.

Including the maximal effects of UV feedback, i.e., $M_{\rm gas} = 0$ and no star formation in all galaxies below the fiducial limit of $M_{\rm min} = 10^9\,M_\odot$ at all z, naturally leads the cut-off shifting to brighter luminosities by about two to three AB magnitudes in all DM models considered: the $z \simeq 7$ LFs for CDM and 3 keV WDM cut-off at $M_{\rm UV} \simeq -12$, while the 1.5 keV LF cuts-off at $M_{\rm UV} \simeq -14$. It is interesting to see that probing down to $M_{\rm UV} \simeq -14.5$, observations are beginning to enter the regime at which the 1.5 keV UV LF cuts-off, though all three DM models including maximal UV feedback are still in agreement with available data sets. However, as shown in Figure 4, roughly 85% of the IGM is ionized by volume at $z \simeq 7$ in the 1.5 keV scenario—this implies that 15% of the volume would still be capable of hosting star formation in halos

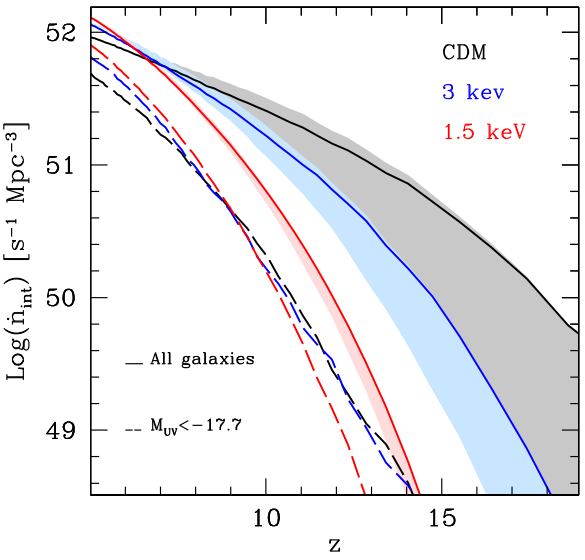

Figure 8. Redshift evolution of the intrinsic ionizing photon emissivity for CDM (black line), 3 keV (blue line), and 1.5 keV (red line) WDM. Solid lines show the fiducial results obtained using Equation (10), where a progressively larger fraction of low-mass ($M_h \lesssim 10^9\,M_\odot$) halos are UV feedback suppressed, with dashed lines showing results for galaxies that have been detected with $M_{\rm UV} \sim -17.7$ (dashed lines). The upper and lower limits of the shaded (black, blue, and red) regions show the SMD range (for CDM, 3, and 1.5 keV WDM) obtained by ignoring and including the effects of UV feedback respectively. The $\dot{n}_{\rm int}$–z relations for different models are quantified in Table 3.

below $M_{\rm min}$, pushing up the LF. Interestingly, the faint end slope remains unchanged for all DM models with $\alpha \simeq -2.04 \pm 0.74$ at $z \simeq 7$, increasing to -2.10 ± 0.62 at $z \simeq 8$ (see also Dayal et al. 2014a), which are in excellent agreement with the values of $\alpha \simeq -2.04^{+0.13}_{-0.17}$ observed at $z \simeq 7$ by Atek et al. (2015) and of $\alpha \simeq -2.07 \pm 0.04\,(-2.02 \pm 0.04)$ observed at $z \simeq 7\,(8)$ by Livermore et al. (2016).

To summarize, CDM and WDM UV LFs overlap over the entire observed range and therefore cannot be used to rule out WDM models even using the faintest galaxies with $M_{\rm UV} \simeq -14.5$ detected so far, corresponding to halo masses of $M_h \simeq 10^{9\text{–}9.5}\,M_\odot$. Furthermore, the exact magnitude at which the LF cuts off depends both on the DM model as well as the feedback prescription implemented—indeed, the 1.5 keV LF excluding UV feedback is essentially degenerate with that obtained in CDM including the effects of both SN and UV feedback.

4.2. Ionizing Photon Density

The intrinsic ionizing photon density and its z-evolution is a key input for modeling reionization. We start by comparing $\dot{n}_{\rm int}$ obtained from the different DM models considering three scenarios, each of which includes SN feedback: (a) ignoring UV feedback, i.e., $M_{\rm min} = 0$, (b) including maximal UV feedback, i.e., $M_{\rm gas} = 0$ in halos with $M_h \lesssim M_{\rm min}$, and (c) the more realistic case where we only suppress the gas mass of galaxies with $M_h \lesssim M_{\rm min}$ in ionized regions. We model the third case as

$$\dot{n}_{\rm int}(z) = \dot{n}_{\rm int,ufb} Q_{\rm II} + \dot{n}_{\rm int,noufb}(1 - Q_{\rm II}). \quad (10)$$

Here, $\dot{n}_{\rm int,ufb}$ and $\dot{n}_{\rm int,noufb}$ represent the ionizing photon production rates including and ignoring UV feedback, respectively. This formalism leads to a situation where a progressive fraction of $M_h \lesssim M_{\rm min}$ galaxies are photo-heating suppressed. UV feedback suppresses the largest amount of star formation and hence $\dot{n}_{\rm int}$ in CDM—as shown in Figure 8, including UV feedback decreases $\dot{n}_{\rm int}$ by about order of magnitude in the initial reionization stages at $z \gtrsim 15$. With a smaller number of low-mass halos, $\dot{n}_{\rm int}$ is suppressed by a factor of three in 3 keV WDM at the same redshifts, while 1.5 keV WDM galaxies are essentially impervious to this effect. The $\dot{n}_{\rm int}$–z evolution for the fiducial model described in Equation (10) is tabulated in Table 3. As noted in Section 3.2, the delay in structure formation, and hence the intrinsic production of ionizing photons, in the 1.5 keV WDM model can be compensated by a larger $f_{\rm esc}$ at earlier epochs. Finally, we find that including/excluding UV feedback has no effect on $\dot{n}_{\rm int}$ for the massive galaxies that have been observed with $M_{\rm UV} \lesssim -17.7$. Their large masses also result in a minimal dependence on the DM model, as shown in Figure 8 and tabulated in Table 3.

4.3. Stellar Mass Density

Encoding information on the entire stellar mass assembled at any cosmic epoch, the SMD and its z-evolution is a key test of theoretical models. We discuss the SMD–z relation considering the three key scenarios described in Section 4.3 above—no UV feedback, full baryonic suppression in galaxies with $M_h \lesssim M_{\rm min}$ and the realistic scenario wherein

$$\mathrm{SMD}(z) = \mathrm{SMD}_{\rm ufb} Q_{\rm II} + \mathrm{SMD}_{\rm noufb}(1 - Q_{\rm II}). \quad (11)$$

Here $\mathrm{SMD}_{\rm ufb}$ and $\mathrm{SMD}_{\rm noufb}$ represent the total SMD calculated using the maximal UV feedback scenario (case B above) and ignoring UV feedback (case A above), respectively. This formalism leads to a realistic situation where no galaxies are UV feedback suppressed in the initial reionization stages, where $Q_{\rm II} \ll 1$. As reionization progresses, a progressively larger fraction of galaxies below $M_{\rm min}$ are UVB suppressed, culminating in all such galaxies being fully suppressed when $Q_{\rm II} \to 1$. The results of these calculations for all galaxies at any z are shown in the left panel in Figure 9—as expected, including UV feedback has the largest effect on the SMD in the initial reionization stages for CDM, given that it contains the largest number of low-mass halos below $M_{\rm min}$. The effect of UV feedback reduces with decreasing redshift since such low-mass halos lose most/all of their gas mass after a single epoch of star formation, according to our formalism. The importance of UV feedback on the SMD naturally reduces with decreasing m_x in WDM models given the dearth of low-mass halos. As seen from the same plot, while the SMD decreases by about an order of magnitude by including UV feedback for CDM, it only changes by about 0.5 (0.2) magnitudes for three (1.5) keV WDM. The SMD–z relation for all the above mentioned cases is detailed in Table 3. As is clearly seen, the slope of the SMD–z relation is extremely steep for the 1.5 keV model compared to CDM or 3 keV. As noted in Dayal et al. (2014b), these relations are independent of the free-parameter (star-formation efficiency threshold and fraction of SN energy coupling to winds) values used. Indeed, in the same work, the authors have shown that with its capability of pinning down the slope evolution of the SMD down to $M_{\rm UV} \simeq -16.5$, the *JWST* will be invaluable in differentiating between CDM and 1.5 keV WDM cosmologies.

Finally, we check that the SMD from all three DM models are in accord with observed data, as shown in the right panel of the same figure. The observed SMDs have been inferred by

Table 3
Relations between Different Quantities for the Three DM Models Considered

DM Model	SN Feedback	UVB Feedback	UV Cut	$\dot{n}_{\rm int}$–M_* Relation at $z \simeq 7$
CDM	yes	no	all galaxies	$\log(\dot{n}_{\rm int}) = \log(M_*) + 45$
3 keV WDM	yes	no	all galaxies	$\log(\dot{n}_{\rm int}) = 0.98\log(M_*) + 45$
1.5 keV WDM	yes	no	all galaxies	$\log(\dot{n}_{\rm int}) = 0.88\log(M_*) + 46$
CDM	yes	yes	all galaxies	$\log(\dot{n}_{\rm int}) = 0.95\log(M_*) + 46$
3 keV WDM	yes	yes	all galaxies	$\log(\dot{n}_{\rm int}) = 0.91\log(M_*) + 46$
1.5 keV WDM	yes	yes	all galaxies	$\log(\dot{n}_{\rm int}) = 0.85\log(M_*) + 47$
DM Model	SN Feedback	UVB Feedback	UV Cut	SMD–z Relation
CDM	yes	no	all galaxies	$\log(\rm SMD) = -0.0038z^2 - 0.16z + 8.2$
CDM	yes	yes	all galaxies	$\log(\rm SMD) = -0.0086z^2 - 0.16z + 8.2$
CDM	yes	yes	all galaxies (Equation (11))	$\log(\rm SMD) = -0.0015z^2 - 0.21z + 8.2$
3 keV	yes	no	all galaxies	$\log(\rm SMD) = -0.011z^2 - 0.18z + 8.4$
3 keV	yes	yes	all galaxies	$\log(\rm SMD) = -0.006z^2 - 0.2z + 8.4$
3 keV	yes	yes	all galaxies (Equation (11))	$\log(\rm SMD) = -0.0032z^2 - 0.25z + 8.6$
1.5 keV	yes	no	all galaxies	$\log(\rm SMD) = -0.02z^2 - 0.13z + 8.4$
1.5 keV	yes	yes	all galaxies	$\log(\rm SMD) = -0.02z^2 - 0.14z + 8.4$
1.5 keV	yes	yes	all galaxies (Equation (11))	$\log(\rm SMD) = -0.017z^2 - 0.16z + 8.4$
CDM	yes	yes	$M_{\rm UV} \lesssim -17.7$	$\log(\rm SMD) = -0.011z^2 - 0.23z + 8.4$
3 keV	yes	yes	$M_{\rm UV} \lesssim -17.7$	$\log(\rm SMD) = -0.014z^2 - 0.21z + 8.4$
1.5 keV keV	yes	yes	$M_{\rm UV} \lesssim -17.7$	$\log(\rm SMD) = -0.026z^2 - 0.085z + 8.1$
DM Model	SN Feedback	UVB Feedback	UV Cut	M_*/M_h–z Relation
CDM	yes	no	$M_{\rm UV} \lesssim -16.5$	$\log(M_*/M_h) = -0.0031z^2 - 0.018z - 1.7$
CDM	yes	no	$M_{\rm UV} \lesssim -17.7$	$\log(M_*/M_h) = -0.0031z^2 - 0.08z - 1.6$
1.5 keV	yes	no	$M_{\rm UV} \lesssim -16.5$	$\log(M_*/M_h) = -0.0054z^2 - 0.012z - 1.4$
1.5 keV	yes	no	$M_{\rm UV} \lesssim -17.7$	$\log(M_*/M_h) = -0.0041z^2 - 0.01z - 1.4$
CDM	yes	yes	$M_{\rm UV} \lesssim -16.5$	$\log(M_*/M_h) = -0.0015z^2 - 0.07z - 1.7$
CDM	yes	yes	$M_{\rm UV} \lesssim -17.7$	$\log(M_*/M_h) = -0.0021z^2 - 0.08z - 1.6$
1.5 keV	yes	yes	$M_{\rm UV} \lesssim -16.5$	$\log(M_*/M_h) = -0.0051z^2 - 0.013z - 1.4$
1.5 keV	yes	yes	$M_{\rm UV} \lesssim -17.7$	$\log(M_*/M_h) = -0.004z^2 - 0.011z - 1.4$

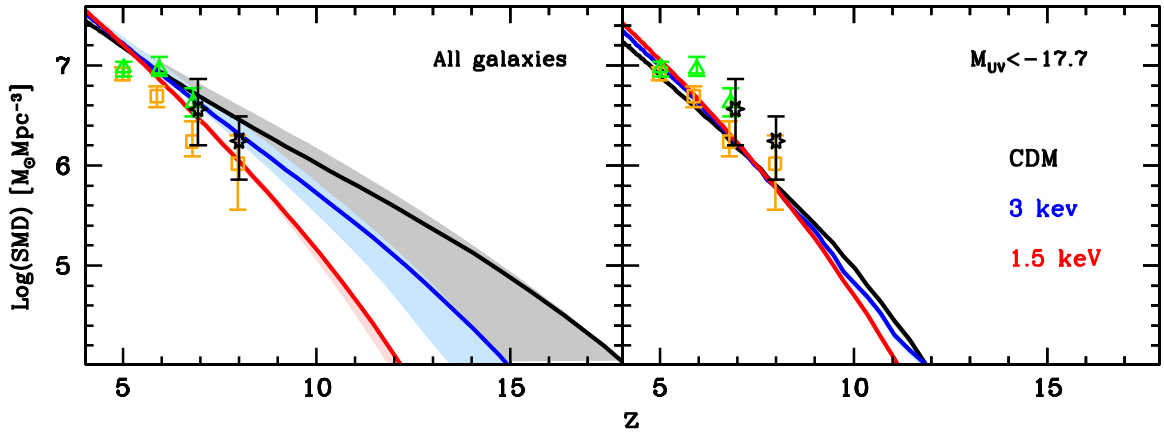

Figure 9. SMD as a function of z for CDM (black line), 3 keV (blue line), and 1.5 keV (red line) WDM for all galaxies (left panel) and galaxies that have been detected (right panel). The upper and lower limits of the shaded (black, blue, and red) regions show the SMD range (for CDM, 3, and 1.5 keV WDM) obtained by ignoring and including the effects of UV feedback respectively. The solid lines show the fiducial results obtained using Equation (11), where a progressively larger fraction of low-mass ($M_h \lesssim 10^9\,M_\odot$) halos are UV feedback suppressed. As seen in the right panel, the SMDs from all three models are in accord for the massive galaxies ($M_{\rm UV} \leqslant -17.7$) that have already been observed, as shown by data points: González et al. (2011, empty triangles), Stark et al. (2013, empty squares), and Labbé et al. (2010a, 2010b, empty stars).

integrating down to a limit of $M_{\rm UV} \lesssim -17.7$. As expected, these galaxies, corresponding to $M_h \lesssim 10^{10.5}\,M_\odot$, are large enough to be impervious to the effects of UV feedback, as a result of which $\rm SMD_{ufb} \simeq SMD_{noufb}$. The theoretical SMD–$z$ relations for observed galaxies are also tabulated in Table 3.

4.4. Stellar Mass–Halo Mass Relations

We now discuss the relation between the stellar and halo mass for high-z galaxies for the three DM models considered as shown in Figure 10. As expected, the value of M_*/M_h increases with increasing halo mass for all models for

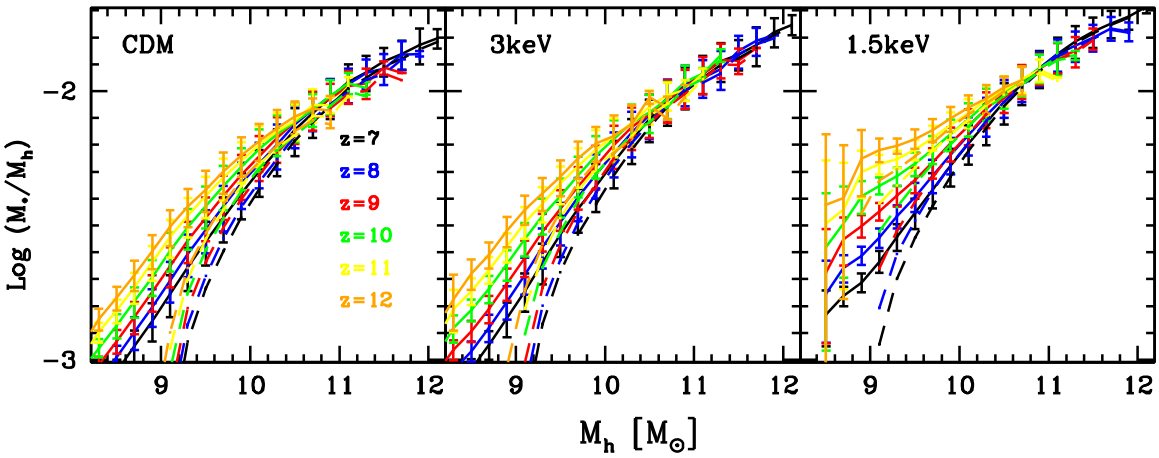

Figure 10. M_*/M_h relation as a function of halo mass for CDM (left panel), 3 keV (central panel), and 1.5 keV WDM (right panel) for the redshifts marked. In each panel, solid and dashed lines show results considering only SN feedback and the complete fiducial model (SN and UV feedback), respectively; we show $1-\sigma$ errors for the former case. As seen, the M_*/M_h relation for low-mass ($M_h \lesssim 10^{10}\,M_\odot$) halos decreases in amplitude with decreasing redshift as a result of feedback progressively decreasing the gas mass, and hence star-forming capabilities, of such halos; the relation converges for larger halo masses signifying the low importance of feedback on such massive systems. See Section 4.4 for details.

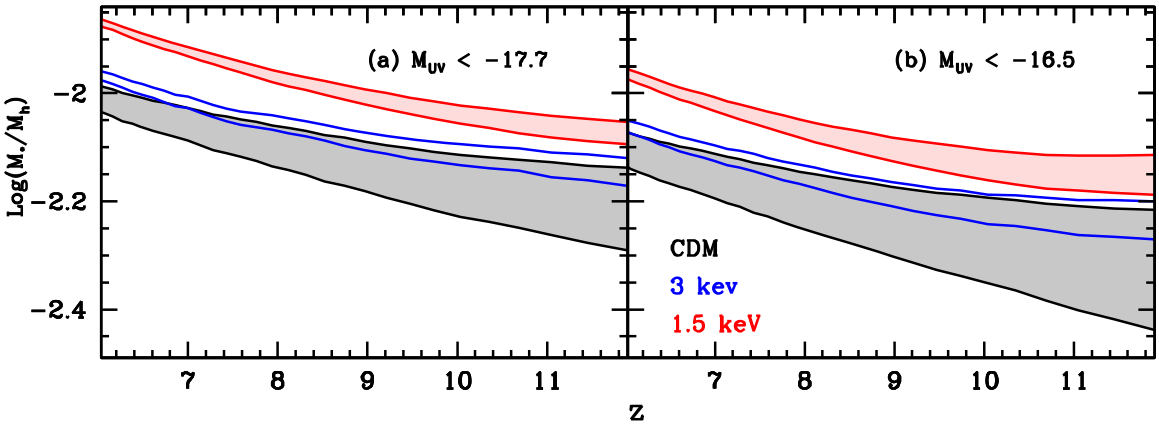

Figure 11. M_*/M_h relation as a function of z for CDM (black lines), 3 keV WDM (blue lines), and 1.5 keV WDM (red lines) integrating down to a UV magnitude corresponding to −17.7 (observed galaxies) and −16.5 in the eft and right panels, respectively. In each panel, the top and bottom lines show the relation ignoring and including UV feedback, for each DM model. As seen, the steeper slope of the M_*/M_h–z relation could be used to obtain constraints on the WDM particle mass.

$z \simeq 7$–12, signifying their larger star-formation efficiencies. Starting by ignoring UVB feedback, in CDM, $z \simeq 7$ $M_h \simeq 10^9\,M_\odot$ galaxies have $M_*/M_h \simeq 0.2\%$—this rises by a factor of about 7 to 1.4% for $10^{11.5}\,M_\odot$ halos, with the slope flattening off above this value. While the M_*/M_h value is independent of z for $M_h \gtrsim 10^{10.5}$ galaxies, corresponding to $M_{\rm UV} \lesssim -17$, M_*/M_h decreases with decreasing z for lower mass halos by about 0.3 dex from $z \simeq 12$ to 7. This is a result of SN-driven winds progressively decreasing the gas mass, and hence star-formation capabilities, in low-mass halos through time. While a similar behavior is observed for $M_h \gtrsim 10^{10.5}$ galaxies in 1.5 keV WDM, lower mass galaxies exhibit higher M_*/M_h values at earlier cosmic epochs as a result of the larger (initial) potential wells—M_*/M_h rises from about 0.2% at $z \simeq 7$ to about 0.6% at $z \simeq 12$ for $M_h \simeq 10^9\,M_\odot$ galaxies in this model, compared to the marginal rise from 0.2% to 0.3% seen in CDM at the same redshifts.

Including the maximal UV feedback scenario (i.e., $M_{\rm gas} = 0$ for $M_h \lesssim 10^9\,M_\odot$ halos) naturally results in a decrease in the M_*/M_h ratio for low-mass halos since their (gas devoid) progenitors are unable to form stars and build up their stellar content. This results in the M_*/M_h values of low-mass ($M_h \lesssim 10^{9.5}\,M_\odot$) galaxies decreasing by about 0.3 dex in CDM and about 0.15 dex for 1.5 keV WDM at $z \simeq 12$. We find that the effect of UV feedback loses its impact with decreasing z as a result of low-mass progenitors losing gas due to SN feedback. While WDM galaxies show the same trends of M_*/M_h with halo mass and z, there are quantitative differences: first, the M_*/M_h trend does not show any flattening at large masses, which is a result of galaxies starting from larger and hence less feedback limited progenitors in such models compared to CDM. Second, at a given halo mass, while the CDM and 3 keV M_*/M_h relations are quite similar, the amplitude of this relation is higher by about 0.2–0.4 dex in the 1.5 keV scenario, which is again driven by the fact that starting from larger progenitors, galaxies of a given halo mass are less feedback limited and hence able to assemble larger stellar masses. We end by noting that the "true" stellar mass value should lie between these limits of zero and maximal UV feedback; while most low-mass galaxies would be unaffected by UV feedback in the initial reionization stages, the results would move closer to the maximal UV feedback scenario in the end reionization stages.

We then study the z-evolution of the M_*/M_h relation in different DM cosmologies, shown in Figure 11. As seen from this plot, CDM shows the lowest M_*/M_h value at any z—this is

the result of stronger feedback decreasing the total stellar mass of low-mass halos. As expected, the M_*/M_h value increases with decreasing m_x at any redshift. Indeed, integrating down to a limit of $M_{\rm UV} \simeq -17.7$, CDM galaxies show a M_*/M_h–z slope proportional to $0.003z^2$ ($0.002z^2$) including (excluding) UV feedback. The corresponding, steeper, 1.5 keV WDM slopes have a value of about $0.004z^2$, given the minimal effect of UV feedback on galaxies in this model. As expected, the slopes steepen in all cases integrating down to a fainter magnitude limit of $M_{\rm UV} = -16.5$. In this case, the CDM slopes correspond to $0.003z^2$ ($0.0015z^2$) with (without) UV feedback, which steepens to $0.005z^2$ for the 1.5 keV model as tabulated in Table 3. Current estimates on the stellar mass have an error of about 0.3 dex, with abundance matching techniques, to infer halo masses, resulting in errors of the order of 0.5 dex. While current stellar mass–halo mass observations are probably unable to distinguish between these different slopes, more precise estimates, of both stellar and halo masses, in the future might offer a useful tool to distinguish between CDM and 1.5 keV WDM.

5. Conclusions and Discussion

Although the CDM paradigm has been enormously successful in explaining the large-scale structure of the universe, it shows a number of small-scale problems that can be alleviated by invoking (keV) WDM particles that erase small-scale power, suppressing the formation of low-mass structures. We use a semi-analytic model that traces the DM and baryonic assembly of high-z ($z \simeq 5$–20) galaxies in four DM cosmologies—CDM and WDM with $m_x = 1.5$, 3, and 5 keV—including the key baryonic processes of star formation, SN feedback, and the merger/accretion/ejection driven evolution of gas and stellar mass. This model uses only two *z- and mass-independent free parameters* with fiducial values of 3.8% for the maximum star-formation efficiency and 10% of the SN energy going into unbinding gas (Dayal et al. 2014a, 2014b). Modeling reionization requires an additional free parameter, which is the fraction of ionzing photons that can escape out of the galactic environment, $f_{\rm esc}$. In this work, we also include the effects of external feedback from a UVB suppressing the baryonic content of galaxies below a threshold mass, for which we use a fiducial value of $M_h \simeq 10^9\,M_\odot$. The model is constrained using key observables for high-z galaxies (UV LF, SMD, *M/L* ratios), the latest constraints on the cosmological electron scattering optical depth ($\tau_{\rm es}$) from *Planck* and the measured ionizing photon emissivity ($\dot{n}_{\rm ion}$) to understand: (1) the reionization history and sources and (2) the effects of UV feedback on galaxy assembly in different DM cosmologies. Our main findings can be summarized as follows.

1. Simultaneously matching $\tau_{\rm es}$ and $\dot{n}_{\rm ion}$ requires a z-dependent $f_{\rm esc} \propto (1+z)^{\alpha}$. Although 1.5 keV WDM requires an exceptionally steep z-dependence, compared to the other models, the latest $\tau_{\rm es}$ estimates (Planck Collaboration et al. 2016a, 2016b) allow the DM mass to range from Gev for CDM to 1.5 keV WDM.
2. Although the start of the reionization process is delayed in light WDM models, a faster galaxy assembly and a steeper redshift dependence of $f_{\rm esc}$ result in reionization ending at almost the same epoch $z \simeq 5.5$–6 in all DM models (see also Yue & Chen 2012). In terms of reionization sources, the bulk of the reionization photons come from galaxies with $M_h \lesssim 10^9\,M_\odot$ and $-10 \lesssim M_{\rm UV} \lesssim -15$ in CDM. The progressive suppression of low-mass halos in light WDM models results in a shift in the reionization population to larger halo masses of $M_h \gtrsim 10^9\,M_\odot$ and $-13 \lesssim M_{\rm UV} \lesssim -17$ for $m_x = 1.5$ keV WDM.
3. We quantify the effects of UV feedback on observables including the evolving UV LF, SMD, $\dot{n}_{\rm int}$, and the M_*/M_h ratio and show that its effects are the most pronounced for CDM (with the largest number of low-mass halos) and decrease with a decreasing WDM particle mass. We find that even in the maximal UV feedback scenario (where $M_h \lesssim 10^9\,M_\odot$ galaxies have no gas content), all DM models (CDM, 3, and 1.5 keV WDM) are in agreement with each other down to the current observational limits of $M_{\rm UV} \simeq -14.5$.
4. Interestingly, the UV LFs obtained from the different DM models considered are degenerate with the physics implemented—for example, the 1.5 keV LF excluding UV feedback is indistinguishable from that obtained in CDM, including the effects of both SN and UV feedback. We find that the SMD and $\dot{n}_{\rm ion}$ values are indistinguishable among the different DM models for observed galaxies, with the differences being the most pronounced for the smallest halos.
5. We find that, in addition to the slope of the SMD–z relation, which will be measured with the forthcoming *JWST* (Dayal et al. 2014b), another global estimate is the redshift evolution of the M_*/M_h relation that can potentially be used to put constraints on the DM particle mass.

We end with a few caveats. First, we have assumed reionization to be solely driven by the stars within galaxies. In recent times, it has been proposed that a population of relatively faint quasars at high-z can complete reionization without any significant contribution from galaxies (Madau & Haardt 2015; Mitra et al. 2015; D'Aloisio et al. 2016; Khaire et al. 2016). It would be interesting to explore the contribution of these quasars in the framework of the WDM models and see if these objects can relax the rapidly evolving $f_{\rm esc}$ required from 1.5 keV WDM models. Second, we have ignored SN radiative losses that could significantly reduce the total energy available to drive winds. However, a decrease in this total energy could be countered by scaling up the fraction of the total energy we put into driving winds from the fiducial value of 10% used in this work. Third, Pawlik et al. (2009) have shown that UVB photo-heating reduces the clumping factor of the IGM since the additional pressure support from reionization smoothes out small scale density fluctuations. While we have used their results for an over-density of 100, we have confirmed that our results do not change using threshold values of 50 or 200. Fourth, while we assume that all halos with mass $M_h \lesssim 10^9\,M_\odot$ are feedback suppressed, we find that our results are equally consistent with observations ($\tau_{\rm es}$ and $\dot{n}_{\rm ion}$) using values ranging between $10^{8.5}$ and $10^{9.5}\,M_\odot$. Finally, we have made the simplifying assumption of using a mass-independent $f_{\rm esc}$ at all z. This is partly motivated by the uncertainty regarding the mass-dependence of $f_{\rm esc}$: while some authors find $f_{\rm esc}$ to decrease with an increase in the halo mass (Razoumov & Sommer-Larsen 2010; Yajima et al. 2011; Ferrara & Loeb 2013), other works have found the opposite trend (Gnedin et al. 2008; Wise & Cen 2009). Significant progress is

expected to be made by comparing our model predictions with further LBG data expected from the Frontier Fields, and from forthcoming observatories such as the *JWST*. Furthermore, if the claim of 3.5 keV X-ray line holds to be true, it will usher in an exciting era for WDM dominated cosmology.

P.D. acknowledges support from the European Commission's CO-FUND Rosalind Franklin program. V.B. acknowledges support from NSF grant AST-1413501. F.P. acknowledges the SAO *Chandra* grant AR6-17017B and NASA-ADAP grant MA160009. P.D. and T.R.C. thank the Sexten Centre for Astrophysics for their hospitality, where a part of this work was carried out. The authors thank A. Taylor and M. Viel for helpful discussions and A. Mazumdar for help with understanding the particle physics aspect of WDM.

References

Ade, P. A. R., Aghanim, N., Armitage-Caplan, C., et al. (Planck Collaboration) 2014a, A&A, 571, A1
Ade, P. A. R., Aghanim, N., Armitage-Caplan, C., et al. (Planck Collaboration) 2014b, A&A, 571, A16
Ade, P. A. R., Aghanim, N., Armitage-Caplan, C., et al. (Planck Collaboration) 2016a, A&A, 594, 13
Ade, P. A. R., Aghanim, N., Armitage-Caplan, C., et al. (Planck Collaboration) 2016b, A&A, 596, 107
Atek, H., Richard, J., Jauzac, M., et al. 2015, ApJ, 814, 69
Barkana, R., Haiman, Z., & Ostriker, J. P. 2001, ApJ, 558, 482
Barkana, R., & Loeb, A. 2001, PhR, 349, 125
Benson, A. J., Farahi, A., Cole, S., et al. 2013, MNRAS, 428, 1774
Blumenthal, G. R., Faber, S. M., Primack, J. R., & Rees, M. J. 1984, Natur, 311, 517
Bode, P., Ostriker, J. P., & Turok, N. 2001, ApJ, 556, 93
Bond, J. R., & Szalay, A. S. 1983, ApJ, 274, 443
Bouwens, R. J., Illingworth, G. D., González, V., et al. 2010, ApJ, 725, 1587
Bouwens, R. J., Illingworth, G. D., Oesch, P. A., et al. 2011, ApJ, 737, 90
Bouwens, R. J., Illingworth, G. D., Oesch, P. A., et al. 2015b, ApJ, 803, 34
Bouwens, R. J., Oesch, P. A., Labbé, I., et al. 2016, ApJ, 830, 67
Bouwens, R. J., Smit, R., Labbe, I., et al. 2015a, arXiv
Bowler, R. A. A., Dunlop, J. S., McLure, R. J., et al. 2014, MNRAS, 440, 2810
Bowler, R. A. A., Dunlop, J. S., McLure, R. J., et al. 2015, MNRAS, 452, 1817
Boyarsky, A., Ruchayskiy, O., Iakubovskyi, D., & Franse, J. 2014, PhRvL, 113, 251301
Boylan-Kolchin, M., Bullock, J. S., & Kaplinghat, M. 2012, MNRAS, 422, 1203
Bradley, L. D., Trenti, M., Oesch, P. A., et al. 2012, ApJ, 760, 108
Bradley, L. D., Zitrin, A., Coe, D., et al. 2014, ApJ, 792, 76
Bromm, V., & Yoshida, N. 2011, ARA&A, 49, 373
Bulbul, E., Markevitch, M., Foster, A., et al. 2014, ApJ, 789, 13
Castellano, M., Fontana, A., Paris, D., et al. 2010, A&A, 524, A28
Choudhury, T. R., & Ferrara, A. 2007, MNRAS, 380, L6
Choudhury, T. R., Ferrara, A., & Gallerani, S. 2008, MNRAS, 385, L58
Ciardi, B., & Ferrara, A. 2005, SSRv, 116, 625
Cole, S., Percival, W. J., Peacock, J. A., et al. 2005, MNRAS, 362, 505
D'Aloisio, A., Upton Sanderbeck, P. R., McQuinn, M., Trac, H., & Shapiro, P. R. 2016, arXiv:1607.06467
Dayal, P., Ferrara, A., Dunlop, J. S., & Pacucci, F. 2014a, MNRAS, 445, 2545
Dayal, P., Mesinger, A., & Pacucci, F. 2014b, arXiv:1408.1102
de Souza, R. S., Mesinger, A., Ferrara, A., et al. 2013, MNRAS, 432, 3218
de Vega, H. J., & Sanchez, N. G. 2010, MNRAS, 404, 885
Ferrara, A., & Loeb, A. 2013, MNRAS, 431, 2826
Garzilli, A., Boyarsky, A., & Ruchayskiy, O. 2015, arXiv:1510.07006
Gnedin, N. Y., Kravtsov, A. V., & Chen, H.-W. 2008, ApJ, 672, 765
González, V., Labbé, I., Bouwens, R. J., et al. 2011, ApJL, 735, L34
Haardt, F., & Madau, P. 2012, ApJ, 746, 125
Hinshaw, G., Larson, D., Komatsu, E., et al. 2013, ApJS, 208, 19
Kang, X., Macciò, A. V., & Dutton, A. A. 2013, ApJ, 767, 22
Khaire, V., Srianand, R., Choudhury, T. R., & Gaikwad, P. 2016, MNRAS, 457, 4051
Klypin, A., Kravtsov, A. V., Valenzuela, O., & Prada, F. 1999, ApJ, 522, 82
Kuhlen, M., & Faucher-Giguere, C.-A. 2012, MNRAS, 423, 862
Labbé, I., González, V., Bouwens, R. J., et al. 2010a, ApJL, 716, L103
Labbé, I., González, V., Bouwens, R. J., et al. 2010b, ApJL, 708, L26
Lange, A. E., Ade, P. A., Bock, J. J., et al. 2001, PhRvD, 63, 042001
Leitherer, C., Schaerer, D., Goldader, J. D., et al. 1999, ApJS, 123, 3
Livermore, R. C., Finkelstein, S. L., & Lotz, J. M. 2016, arXiv:1604.06799
Macciò, A. V., Paduroiu, S., Anderhalden, D., Schneider, A., & Moore, B. 2012, MNRAS, 424, 1105
Madau, P., & Haardt, F. 2015, ApJL, 813, L8
Madau, P., Haardt, F., & Rees, M. J. 1999, ApJ, 514, 648
Magg, M., Hartwig, T., Glover, S. C. O., Klessen, R. S., & Whalen, D. J. 2016, MNRAS, 462, 3591
McLeod, D. J., McLure, R. J., & Dunlop, J. S. 2016, MNRAS, 459, 3812
McLure, R. J., Dunlop, J. S., Bowler, R. A. A., et al. 2013, MNRAS, 432, 2696
McLure, R. J., Dunlop, J. S., Cirasuolo, M., et al. 2010, MNRAS, 403, 960
Mitra, S., Choudhury, T. R., & Ferrara, A. 2011, MNRAS, 413, 1569
Mitra, S., Choudhury, T. R., & Ferrara, A. 2012, MNRAS, 419, 1480
Mitra, S., Choudhury, T. R., & Ferrara, A. 2015, MNRAS, 454, L76
Mitra, S., Ferrara, A., & Choudhury, T. R. 2013, MNRAS, 428, L1
Moore, B., Quinn, T., Governato, F., Stadel, J., & Lake, G. 1999, MNRAS, 310, 1147
Navarro, J. F., Frenk, C. S., & White, S. D. M. 1997, ApJ, 490, 493
Oesch, P. A., Bouwens, R. J., Illingworth, G. D., et al. 2010, ApJL, 709, L16
Oesch, P. A., Bouwens, R. J., Illingworth, G. D., et al. 2013, ApJ, 773, 75
Oesch, P. A., Brammer, G., van Dokkum, P. G., et al. 2016, ApJ, 819, 129
Pacucci, F., Mesinger, A., & Haiman, Z. 2013, MNRAS, 435, L53
Parkinson, H., Cole, S., & Helly, J. 2008, MNRAS, 383, 557
Pawlik, A. H., Schaye, J., & van Scherpenzeel, E. 2009, MNRAS, 394, 1812
Peebles, P. J. E. 1971, Physical Cosmology (Princeton, NJ: Princeton Univ. Press)
Razoumov, A. O., & Sommer-Larsen, J. 2010, ApJ, 710, 1239
Robertson, B. E., Ellis, R. S., Furlanetto, S. R., & Dunlop, J. S. 2015, ApJL, 802, L19
Schneider, A., Anderhalden, D., Macciò, A. V., & Diemand, J. 2014, MNRAS, 441, L6
Schultz, C., Oñorbe, J., Abazajian, K. N., & Bullock, J. S. 2014, arXiv:1401.3769
Shapiro, P. R., & Giroux, M. L. 1987, ApJL, 321, L107
Sheth, R. K., & Tormen, G. 1999, MNRAS, 308, 119
Slosar, A., Iršič, V., Kirkby, D., et al. 2013, JCAP, 4, 26
Somerville, R. S. 2002, ApJL, 572, L23
Somerville, R. S., Bullock, J. S., & Livio, M. 2003, ApJ, 593, 616
Songaila, A., & Cowie, L. L. 2010, ApJ, 721, 1448
Stark, D. P., Schenker, M. A., Ellis, R., et al. 2013, ApJ, 763, 129
Subramanian, K., Cen, R., & Ostriker, J. P. 2000, ApJ, 538, 528
Teyssier, R., Pontzen, A., Dubois, Y., & Read, J. I. 2013, MNRAS, 429, 3068
Viel, M., Becker, G. D., Bolton, J. S., & Haehnelt, M. G. 2013, PhRvD, 88, 043502
Viel, M., Lesgourgues, J., Haehnelt, M. G., Matarrese, S., & Riotto, A. 2005, PhRvD, 71, 063534
Weinberg, D. H., Bullock, J. S., Governato, F., Kuzio de Naray, R., & Peter, A. H. G. 2015, PNAS, 112, 12249
Wise, J. H., & Cen, R. 2009, ApJ, 693, 984
Wyithe, J. S. B., & Bolton, J. S. 2011, MNRAS, 412, 1926
Wyse, R. F. G. 2001, in ASP Conf. Ser. 230, Galaxy Disks and Disk Galaxies, ed. J. G. Funes & E. M. Corsini (San Francisco, CA: ASP), 71
Yajima, H., Choi, J.-H., & Nagamine, K. 2011, MNRAS, 412, 411
Yoshida, N., Sokasian, A., Hernquist, L., & Springel, V. 2003, ApJL, 591, L1
Yue, B., & Chen, X. 2012, ApJ, 747, 127
Zheng, W., Postman, M., Zitrin, A., et al. 2012, Natur, 489, 406